Papoulis-Gerchberg Algorithms for Limited Angle Tomography Using Data Consistency Conditions

Yixing Huang, Oliver Taubmann, Xiaolin Huang, Guenter Lauritsch and Andreas Maier

***Abstract*—The Papoulis-Gerchberg (P-G) algorithm is widely used for extrapolation of band-limited signals. It is applicable to limited angle tomography as well since typical imaged objects in computed tomography have a limited spatial extent, which means that the Fourier transforms of the objects can be considered band-limited signals. In computed tomography, some other band-limitation properties have been discovered as well, which are referred to as data consistency conditions. For example, the Fourier transform of a parallel-beam sinogram has an empty double-wedge region. The Chebyshev-Fourier transform of a parallel-beam sinogram only has nonzero values inside a wedge region and these values form a checkerboard pattern, which is Helgason-Ludwig consistency condition. In this paper, we propose two P-G algorithms to restore missing data in limited angle tomography using the above two consistency conditions. Numerical experiments on the Shepp-Logan phantom demonstrate that they can reduce streaks better than the conventional P-G algorithm.**

I. Introduction

In computed tomography (CT), image reconstruction from data acquired in an insufficient angular range is called limited angle tomography [1]–[3]. It arises when the gantry rotation of a CT system is restricted by other system parts or external obstacles. Because of missing data, artifacts, typically in the form of streaks, will occur in the reconstructed images.

Iterative algorithms with total variation are popular in limited angle tomography [4]–[7]. They incorporate sparsity at the gradient domain of medical images into the reconstruction and hence reduce streak artifacts. However, they are computationally expensive. Recently, deep learning has obtained impressive achivement for streak reduction in limited angle tomography [8]–[10], but it depends heavily on the availability and quality of training data.

Extrapolation/interpolation of the missing data is a common way to deal with data insufficiency. The Papoulis-Gerchberg (P-G) algorithm [11], [12] is well known for extrapolating band-limited signals. In limited angle tomography, according to the central slice theorem, some frequency components of an imaged object are missing. Also, the imaged object has a limited spatial extent, which means that the Fourier transform of the object can be considered a band-limited signal. Therefore, to extrapolate the missing frequency components from the measured ones, the P-G algorithm can be applied [13]–[15]. However, it requires strong *a priori* knowledge in that the object support should be known.

In computed tomography, many data consistency conditions have been discovered. For example, the Fourier transform of a parallel-beam sinogram has an empty double-wedge region [16]. The Helgason-Ludwig consistency condition [17], [18] states that Chebyshev-Fourier transform of a parallel-beam sinogram only has nonzero values inside a wedge region and these values form a checkerboard pattern. These consistency conditions are also band-limitation properties of CT data. Many experiments have demonstrated that consistency conditions are beneficial in restoring missing data [19]–[22]. Therefore, in this paper, we propose two P-G algorithms to restore missing data in limited angle tomography using the above two consistency conditions.

II. Methods

A. General P-G Algorithm

Given a measured segment $g_0(t)$ from a band-limited signal $g(t)$,

$$g_0(t) = \begin{cases} g(t) & |t| \le t_0, \\ 0 & |t| > t_0, \end{cases}$$

a characteristic function of the measurement interval $[-t_0, t_0]$,

$$M_g(t) = \begin{cases} 1 & |t| \le t_0, \\ 0 & |t| > t_0, \end{cases}$$

and a perfect low-pass filter $L(w)$,

$$L(w) = \begin{cases} 1 & |w| < w_c, \\ 0 & |w| > w_c, \end{cases}$$

where w_c is the band limit of $g(t)$, $g(t)$ can be estimated by the following algorithm [11], [12],

$$g^l(t) = g_0(t) + (1 - M_g(t)) \cdot \mathcal{F}_1^{-1}\left(L(w) \cdot \mathcal{F}_1\left(g^{l-1}(t)\right)\right),$$

where $\mathcal{F}_d$ and $\mathcal{F}_d^{-1}$ are the d-dimensional Fourier transform and inverse Fourier transform operators, respectively, $g^l(t)$ is an estimation of $g(t)$ at the l-th iteration, and $g^0(t) = g_0(t)$.

B. Conventional P-G Algorithm Using Object Support

We denote an imaged object by $\boldsymbol{f}(\boldsymbol{x})$. Typically the object has a compact support in the spatial domain, denoted by $\boldsymbol{S}$. A characteristic function for the support $\boldsymbol{S}$ is defined as,

$$L_{\boldsymbol{S}}(\boldsymbol{x}) = \begin{cases} 1 & \boldsymbol{x} \in \boldsymbol{S}, \\ 0 & \text{otherwise.} \end{cases}$$

Y. Huang is with Pattern Recognition Lab, Friedrich-Alexander-University Erlangen-Nuremberg, Erlangen, Germany (e-mail: yixing.yh.huang@fau.de).

O. Taubmann, and A. Maier are with Pattern Recognition Lab, Friedrich-Alexander-University Erlangen-Nuremberg, Erlangen, Germany, and also with Erlangen Graduate School in Advanced Optical Technologies (SAOT), Erlangen, Germany.

X. Huang was with Pattern Recognition Lab, Friedrich-Alexander-University Erlangen-Nuremberg, Erlangen, Germany and now is with Institute of Image Processing and Pattern Recognition, Shanghai Jiao Tong University, Shanghai, China.

G. Lauritsch and O. Taubmann are with Siemens Healthcare GmbH, Forchheim, Germany.

The Fourier transform of the object $\boldsymbol{f}(\boldsymbol{x})$ is denoted by $\boldsymbol{F}(w,\theta)$ in polar coordinates, $\boldsymbol{F}(w,\theta) = \mathcal{F}_2\boldsymbol{f}(\boldsymbol{x})$. According to the symmetry property of the Fourier transform, we have $\mathcal{F}_2\boldsymbol{F}(w,\theta) = 2\pi\boldsymbol{f}(\boldsymbol{x})$. Therefore, $\boldsymbol{F}(w,\theta)$ is a band-limited function as, after applying a Fourier transform to it, its components are nonzero only in S.

In computed tomography, the parallel-beam sinogram of the object $\boldsymbol{f}(\boldsymbol{x})$ is denoted by,

$$p(s,\theta) = \int_{\boldsymbol{x}\cdot\boldsymbol{\theta}=s} \boldsymbol{f}(\boldsymbol{x})\mathrm{d}\boldsymbol{x},$$

where $\boldsymbol{\theta} = (\cos\theta, \sin\theta)$, $\theta \in [0, 2\pi)$ is the direction orthogonal to the X-rays, and $s \in (-\infty, \infty)$ is the detector index. The central slice theorem expresses that,

$$\mathcal{F}_1 p(s,\theta) = \boldsymbol{F}(w,\theta).$$

When the sinogram is measured for the whole angular range $[0,\pi)$, the object $\boldsymbol{f}$ can be reconstructed using the standard filtered back-projection (FBP) reconstruction algorithms. However, in limited angle tomography, the sinogram is measured only in a limited angular range, denoted by $[0,\theta_{\max})$ where $\theta_{\max}$ is the maximum scanned angle, $\theta_{\max} < \pi$. In this case, a double wedge region is missing in $\boldsymbol{F}$, i. e.,

$$\boldsymbol{F}_{\text{limited}}(w,\theta)|_{\theta_{\max}\le\theta<\pi,-\infty<w<\infty} = 0,$$

where $\boldsymbol{F}_{\text{limited}}$ is the measured frequency components of $\boldsymbol{f}$ in limited angle tomography. A characteristic function for the measured region is defined as,

$$M_{\boldsymbol{F}}(w,\theta) = \begin{cases} 1 & \theta \in [0,\theta_{\max}), \\ 0 & \text{otherwise.} \end{cases}$$

Restoring the complete $\boldsymbol{F}(w,\theta)$ from $\boldsymbol{F}_{\text{limit}}(w,\theta)$ can thus be considered as an extrapolation problem of a band-limited function. Therefore, the P-G algorithm can be applied,

$$\begin{aligned}\boldsymbol{F}^l(w,\theta) = \boldsymbol{F}_{\text{limited}}(w,\theta) + (1 - M_{\boldsymbol{F}}(w,\theta))\cdot \\ \mathcal{F}_2^{-1}(L_{\boldsymbol{S}}(\boldsymbol{x})\cdot\mathcal{F}_2\boldsymbol{F}^{l-1}(w,\theta)),\end{aligned} \tag{1}$$

where $\boldsymbol{F}^l(w,\theta)$ is an estimation of $\boldsymbol{F}(w,\theta)$ at the l-th iteration and $\boldsymbol{F}^0(w,\theta) = \boldsymbol{F}_{\text{limited}}$. Note that $\mathcal{F}_2$ and $\mathcal{F}_2^{-1}$ can change position here due to the symmetry property. This conventional P-G algorithm is denoted by P-G_{OS}.

C. P-G Algorithm Using Fourier Property Of Sinograms

The 2-D Fourier transform of a complete parallel-beam sinogram is as follows,

$$\boldsymbol{P}(w,k) = \mathcal{F}_2 p(s,\theta) = \frac{1}{2\pi}\int_0^{2\pi}\int_{-\infty}^{\infty} p(s,\theta)e^{-i(ws+k\theta)}\mathrm{d}s\mathrm{d}\theta.$$

A consistency condition in the sinogram's Fourier space is represented as follows [16],

$$\boldsymbol{P}(w,k) \approx 0 \text{ when } \left|\frac{k}{w}\right| > r_p,$$

where r_p is distance of the farthest point on the object to the isocenter. It means that a double-wedge region of $\boldsymbol{P}(w,k)$ is zero. Hence, $p(s,\theta)$ is a band-limited function. A characteristic function for the double-wedge region is defined as,

$$L_{\boldsymbol{P}}(w,k) = \begin{cases} 0 & \left|\frac{k}{w}\right| > r_p, \\ 1 & \text{otherwise.} \end{cases}$$

In limited angle tomography, we denote the measured sinogram by $p_{\text{limited}}(s,\theta)$, $\theta \in [0,\theta_{\max})$. According to $p(s,\theta) = p(-s,\theta+\pi)$, the limited angle sinogram is extended to a 2π angular range, denoted by $p'_{\text{limited}}(s,\theta)$. A characteristic function for the available part of the sinogram is defined as,

$$M_p(s,\theta) = \begin{cases} 1 & \theta \in [0,\theta_{\max}) \cup \theta \in [\pi,\pi+\theta_{\max}), \\ 0 & \text{otherwise.} \end{cases}$$

To extrapolate/interpolate the missing sinogram, the P-G algorithm can be applied,

$$\begin{aligned}p^l(s,\theta) = p'_{\text{limited}}(s,\theta) + (1 - M_p(s,\theta))\cdot \\ \mathcal{F}_2^{-1}\left(L_{\boldsymbol{P}}(w,k)\cdot\mathcal{F}_2 p^{l-1}(s,\theta)\right),\end{aligned} \tag{2}$$

where $p^l(s,\theta)$ is an estimation of $p(s,\theta)$ at the l-th iteration and $p^0(s,\theta) = p'_{\text{limited}}$. The proposed P-G algorithm using the double-wedge property of sinograms' frequency domain is denoted by P-G_{DW}. It was proposed for defect detector gap compensation of emission CT in [23] and sparse-view CT reconstruction in [19].

D. P-G Algorithm Using HLCC

We define the n-th order moment curve of a parallel-beam sinogram $p(s,\theta)$ as,

$$a_n(\theta) = \int_{-\infty}^{\infty} p(s,\theta)T_n(s)\mathrm{d}s,$$

where $T_n(s) = s^n$ and n is the order of the monomial. The Fourier transform of the moment curve is,

$$b_n(m) = \frac{1}{2\pi}\int_0^{2\pi} a_n(\theta)e^{-im\theta}\mathrm{d}\theta.$$

HLCC [17], [18] tells that,

$$b_n(m) = 0, \quad |m| > n \text{ or } m+n \text{ is odd.} \tag{3}$$

Therefore, the moment curves are band-limited functions. A characteristic function for HLCC is defined as,

$$L_{\text{HLCC}}(n,m) = \begin{cases} 1 & \text{if } |m| \le n \text{ and } m+n \text{ is even,} \\ 0 & \text{otherwise.} \end{cases}$$

When $T_n(s)$ is replaced by orthogonal polynomials, e.g., Chebyshev polynomials or Gegenbauer polynomials, $p(s,\theta)$ can be conveniently restored from $a_n(\theta)$ while $L_{\text{HLCC}}(n,m)$ remains the same. In this paper, we use the Chebyshev polynomial of the second kind,

$$U_n(s) = \frac{\sin\left((n+1)\arccos(s)\right)}{\sqrt{1-s^2}}.$$

$U_n(s)$ is a family of orthogonal polynomials at domain [-1, 1] with the scalar weight $W(s) = (1-s^2)^{1/2}$, i.e.,

$$\int_{-1}^{1} W(s)\cdot U_n(s)\cdot U_{n'}(s)\mathrm{d}s = \begin{cases} 0, & n \ne n' \\ \pi/2, & n = n'. \end{cases}$$

Note that here we normalize the detector index s to a range of [-1, 1]. Thus, an approximate sinogram can be restored by the inverse Chebyshev transform from the moment curves,

$$p_{n_r}(s,\theta) = \frac{2}{\pi}\sum_{n=0}^{n_r} a_n(\theta)\left(W(s)\cdot U_n(s)\right),$$

where n_r is the number of orders used.

In limited angle tomography, the moment curves $a_n(\theta)$ are available only at the angular range of $[0,\theta_{\max})$ and $[\pi,\pi+\theta_{\max})$. The available moment curve is denoted by $a_{n,\text{limited}}(\theta)$. An characteristic function for the available parts is defined as,

$$M_{a_n}(\theta) = \begin{cases} 1 & \theta\in[0,\theta_{\max}) \text{ or } \theta\in[\pi,\pi+\theta_{\max}),\\ 0 & \text{otherwise.}\end{cases}$$

To get $p_{n_r}(s,\theta)$, we need to extrapolate/interpolate the missing parts of $a_n(\theta), n=0,1,2,\ldots,n_r$. Hence, the P-G algorithm can be applied,

$$\begin{aligned} a_n^l(\theta) = a_{n,\text{limited}}(\theta) + (1-M_{a_n}(\theta))\cdot \\ \mathcal{F}_1^{-1}\left(L_{\text{HLCC}}(n,m)\cdot\mathcal{F}_1 a_n^{l-1}(\theta)\right),\end{aligned} \tag{4}$$

where $a_n^l(\theta)$ is an estimation of $a_n\theta$ at the l-th iteration. The proposed P-G algorithm using HLCC is denoted by P-G$_{\text{HLCC}}$.

Papoulis and Gerchberg have shown the convergence of P-G algorithms in the noise-free case [11], [12]. When the frequency band is known accurately, the missing signal can be extrapolated exactly with infinite iterations. However, in the presence of noise or discretization error, the missing signal typically cannot be recovered exactly. In [21], we find that the restoration of high order moment curves is severely ill-posed. The observation that the Fourier coefficients of the moment curves are sparse can be used to overcome the ill-posedness. Therefore, we define a soft-thresholding operator $\mathcal{S}_\tau$,

$$\mathcal{S}_\tau(v) = \begin{cases} v-\tau & v>\tau,\\ 0 & -\tau\le v\le\tau,\\ v+\tau & v<-\tau,\end{cases}$$

where v is the value to be soft-thresholded and τ is a threshold. Eq. (4) is then modified as follows,

$$\begin{aligned} a_n^l(\theta) = a_{n,\text{limited}}(\theta) + (1-M_{a_n}(\theta))\cdot \\ \mathcal{F}_1^{-1}\left(\mathcal{S}_\tau\left(L_{\text{HLCC}}(n,m)\cdot\mathcal{F}_1 a_n^{l-1}(\theta)\right)\right).\end{aligned} \tag{5}$$

Here $\mathcal{S}_\tau$ is applied to the imaginary and real Fourier coefficients element-wise. The proposed P-G algorithm using HLCC and soft-thresholding is denoted by P-G$_{\text{HLCC,ST}}$.

E. Simulation Experiments

To evaluate the performance of the proposed algorithms, experiments on the standard high-contrast Shepp-Logan phantom (Fig. 1) are conducted. The major and minor semi-axes of the outer ellipse of the phantom are 94.2 mm and 70.6 mm, respectively. The attenuation coefficients are converted to Hounsfield scale between [-1000, 3000] HU. A limited angle sinogram is computed analytically in a parallel-beam trajectory. The total scanned angular range is 160° and the angular step is 0.5°. The number of the equal-space detector pixels is 1537 and the detector element size is 0.2 mm. No noise is simulated but discretization error exists. The images are reconstructed using FBP with the Ram-Lak filter. The size of the reconstructed images is 512×512 with an isotropic pixel size of 0.4 mm.

Fig. 1. The Shepp-Logan phantom, window: [-1000, 3400] HU.

For P-G$_{\text{OS}}$, we assume that the support of the ground truth Shepp-Logan phantom is exactly known. For P-G$_{\text{DW}}$, we choose $r_p = 94$ mm, which is the top point of the phantom and can be accurately obtained from the limited angle reconstruction result using FBP. For P-G$_{\text{HLCC}}$ and P-G$_{\text{HLCC,ST}}$, the number of used orders n_r is set to 2414. Empirically, the threshold τ is set to $\tau = 0.5\cdot(1-n/2500)$ for n-th moment curve. For all three algorithms, 1000 iterations are performed.

III. Results And Discussion

The images reconstructed from different algorithms and their absolute difference w. r. t. the image reconstructed from the full data are displayed in Fig. 2. The image reconstructed from the limited angle sinogram using FBP, denoted by $\boldsymbol{f}_{\text{limited}}$, is shown in Fig. 2(a). It suffers from streak artifacts. Especially, the outer boundary is severely distorted on the left and right sides. The image reconstructed from P-G$_{\text{OS}}$, denoted by $\boldsymbol{f}_{\text{OS}}$, is shown in Fig. 2(b). The streaks outside the boundary are totally removed, since strong prior knowledge of the ground truth object support is applied. However, streaks inside the support remain. The image reconstructed from P-G$_{\text{DW}}$, denoted by $\boldsymbol{f}_{\text{DW}}$, is shown in Fig. 2(c). Most streaks outside the boundary are reduced, although the boundary is still a little distorted. Its absolute difference image diff$_{\text{DW}}$ displayed in Fig. 2(h) demonstrates that the streaks inside the boundary are also reduced. Figs. 2(d) and (e) are images reconstructed from P-G$_{\text{HLCC}}$ and P-G$_{\text{HLCC,ST}}$, denoted by $\boldsymbol{f}_{\text{HLCC}}$ and $\boldsymbol{f}_{\text{HLCC,ST}}$ respectively. Most streaks remain in $\boldsymbol{f}_{\text{HLCC}}$ (Fig. 2(d)) since only low order moment curves are restored. On the contrary, most streaks at the boundary in $\boldsymbol{f}_{\text{HLCC,ST}}$ (Fig. 2(e)) are reduced and thus the boundary is reconstructed very well. Streaks inside the boundary of $\boldsymbol{f}_{\text{HLCC,ST}}$ are also reduced, although still some small streaks remain. The root-mean-square errors (RMSEs) of images reconstructed from different algorithm indicate that P-G$_{\text{HLCC,ST}}$ has the best performance with the lowest RMSE of 75 HU.

IV. Conclusion

In this paper, we propose two new P-G algorithms based on consistency conditions, P-G$_{\text{DW}}$ and P-G$_{\text{HLCC}}$/P-G$_{\text{HLCC,ST}}$. P-G$_{\text{DW}}$ uses the band-limitation property of sinograms, i. e., that the 2-D Fourier transform of a sinogram has a double-wedge zero region. P-G$_{\text{HLCC,ST}}$ uses the band-limitation property of moment curves according to HLCC. The conventional

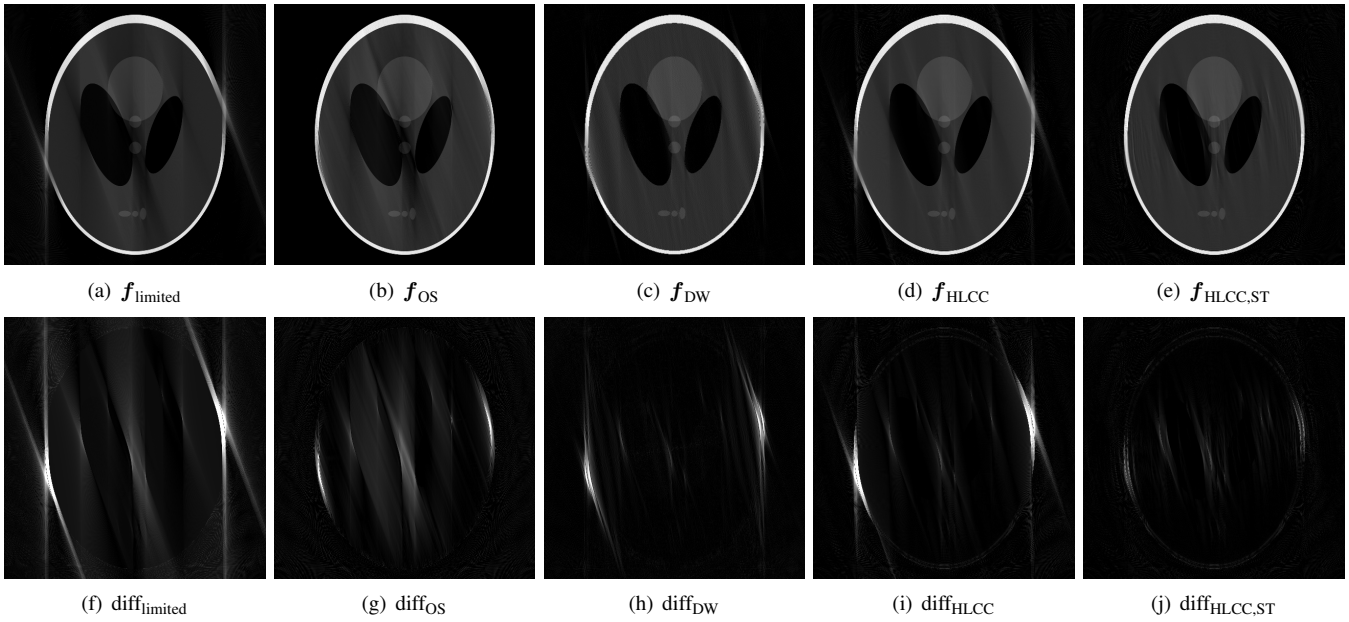

(a) $\boldsymbol{f}_{\text{limited}}$ (b) $\boldsymbol{f}_{\text{OS}}$ (c) $\boldsymbol{f}_{\text{DW}}$ (d) $\boldsymbol{f}_{\text{HLCC}}$ (e) $\boldsymbol{f}_{\text{HLCC,ST}}$

(f) $\text{diff}_{\text{limited}}$ (g) diff_{OS} (h) diff_{DW} (i) $\text{diff}_{\text{HLCC}}$ (j) $\text{diff}_{\text{HLCC,ST}}$

Fig. 2. Reconstructions of the Shepp-Logan phantom using different algorithms and their absolute difference w. r. t. the full data reconstruction. The root-mean square errors for $\boldsymbol{f}_{\text{limited}}$, $\boldsymbol{f}_{\text{OS}}$, $\boldsymbol{f}_{\text{DW}}$, $\boldsymbol{f}_{\text{HLCC}}$, and $\boldsymbol{f}_{\text{HLCC,ST}}$ are 302 HU, 172 HU, 150 HU, 214 HU, and 75 HU, respectively. Window: [-1000, 3400] HU and [-1000, 1000] HU for the top and bottom images, respectively.

P-G algorithm P-G_{OS} requires strong *a priori* knowledge, the exact object support. In contrast, P-G_{DW} only needs the distance of the farthest point, which can be accurately estimated from a limited angle reconstruction. It reduces small streaks inside the boundary better than P-G_{OS}. However, it is unable to reconstruct the boundary well. P-G_{HLCC} only is not sufficient to reduce streaks due to the ill-posedness of high order moment curve extrapolation/interpolation. P-$G_{\text{HLCC,ST}}$ takes the advantage of the sparsity of the Fourier coefficients of the moment curves. It performs the best on streak reduction among the proposed algorithms.

Disclaimer: The concepts and information presented in this paper are based on research and are not commercially available.

REFERENCES

[1] F. A. Grünbaum, "A study of fourier space methods for limited angle image reconstruction," *Numer Funct Anal Optim*, vol. 2, no. 1, pp. 31–42, 1980.

[2] M. E. Davison, "The ill-conditioned nature of the limited angle tomography problem," *SIAM J Appl Math*, vol. 43, no. 2, pp. 428–448, 1983.

[3] E. T. Quinto, "An introduction to x-ray tomography and radon transforms," vol. 63, p. 1, 2006.

[4] E. Sidky, C. Kao, and X. Pan, "Accurate image reconstruction from few-views and limited-angle data in divergent-beam CT," *J Xray Sci Technol*, vol. 14, pp. 119–139, 2006.

[5] Z. Chen, X. Jin, L. Li, and G. Wang, "A limited-angle CT reconstruction method based on anisotropic TV minimization," *Phys Med Biol*, vol. 58, no. 7, pp. 2119–2141, 2013.

[6] Y. Huang, O. Taubmann, X. Huang, V. Haase, G. Lauritsch, and A. Maier, "A new weighted anisotropic total variation algorithm for limited angle tomography," *Procs IEEE ISBI*, pp. 585–588, 2016.

[7] ——, "A new scale space total variation algorithm for limited angle tomography," *Procs CT-Meeting*, pp. 149–152, 2016.

[8] T. Würfl, F. C. Ghesu, V. Christlein, and A. Maier, "Deep learning computed tomography," *Procs MICCAI*, vol. 3, pp. 432–440, 2016.

[9] K. Hammernik, T. Würfl, T. Pock, and A. Maier, "A deep learning architecture for limited-angle computed tomography reconstruction," *Procs BVM*, pp. 92–97, 2017.

[10] J. Gu and J. C. Ye, "Multi-scale wavelet domain residual learning for limited-angle CT reconstruction," *Procs Fully3D*, pp. 443–447, 2017.

[11] R. Gerchberg, "Super-resolution through error energy reduction," *J Mod Opt*, vol. 21, no. 9, pp. 709–720, 1974.

[12] A. Papoulis, "A new algorithm in spectral analysis and band-limited extrapolation," *IEEE Trans Circuits Syst*, vol. 22, no. 9, pp. 735–742, 1975.

[13] G.-r. Qu, Y.-s. Lan, and M. Jiang, "An iterative algorithm for angle-limited three-dimensional image reconstruction," *Acta Math Appl Sin*, vol. 24, no. 1, pp. 157–166, 2008.

[14] G.-r. Qu and M. Jiang, "Landweber iterative methods for angle-limited image reconstruction," *Acta Math Appl Sin*, vol. 25, no. 2, pp. 327–334, 2009.

[15] M. Defrise and C. De Mol, "A regularized iterative algorithm for limited-angle inverse radon transform," *Opt Acta: Int J Opt*, vol. 30, no. 4, pp. 403–408, 1983.

[16] P. R. Edholm, R. M. Lewitt, and B. Lindholm, "Novel properties of the fourier decomposition of the sinogram," *Phys Eng Comput Multidimen Imag Process*, pp. 8–18, 1986.

[17] D. Ludwig, "The Radon transform on Euclidean space," *Comm Pure Appl Math*, vol. 19, no. 1, pp. 49–81, 1966.

[18] S. Helgason, *The Radon transform*. Boston, MA: Birkhauser, 1980.

[19] M. Pohlmann, M. Berger, A. Maier, J. Hornegger, and R. Fahrig, "Estimation of missing fan-beam projections using frequency consistency conditions," *Procs CT Meeting*, pp. 203–207, 2014.

[20] M. Berger, Y. Xia, W. Aichinger, K. Mentl, M. Unberath, A. Aichert, C. Riess, J. Hornegger, R. Fahrig, and A. Maier, "Motion compensation for cone-beam CT using Fourier consistency conditions," *Phys Med Biol*, vol. 62, no. 17, pp. 7181–7215, 2017.

[21] Y. Huang, X. Huang, O. Taubmann, Y. Xia, V. Haase, J. Hornegger, G. Lauritsch, and A. Maier, "Restoration of missing data in limited angle tomography based on Helgason-Ludwig consistency conditions," *Biomed Phys & Eng Express*, vol. 3, no. 3, p. 035015, 2017.

[22] Y. Xia, M. Berger, S. Bauer, S. Hu, A. Aichert, and A. Maier, "An improved extrapolation scheme for truncated CT data using 2D Fourier-based Helgason-Ludwig consistency conditions," *Int J Biomed Imaging*, vol. 2017, 2017.

[23] J. Karp, G. Muehllehner, and R. Lewitt, "Constrained fourier space method for compensation of missing data in emission computed tomography," *IEEE Trans Med Imaging*, vol. 7, no. 1, pp. 21–25, 1988.